SCIENTIFIC REPORTS

OPEN

SUBJECT AREAS:
ANALYTICAL CHEMISTRY
PLASMA PHYSICS

Received
16 July 2014

Accepted
4 December 2014

Published
5 January 2015

Correspondence and requests for materials should be addressed to Y.D. (yduan@scu.edu.cn)

Laser Induced Breakdown Spectroscopy Based on Single Beam Splitting and Geometric Configuration for Effective Signal Enhancement

Guang Yang[1,2], Qingyu Lin[1], Yu Ding[2], Di Tian[2] & Yixiang Duan[1]

[1]Research Center of Analytical Instrumentation, Key Laboratory of Bio-resource and Eco-environment, Ministry of Education, College of Life Science, Sichuan University, Chengdu, China, [2]College of Instrumentation & Electrical Engineering, Jilin University, Changchun, China.

A new laser induced breakdown spectroscopy (LIBS) based on single-beam-splitting (SBS) and proper optical geometric configuration has been initially explored in this work for effective signal enhancement. In order to improve the interaction efficiency of laser energy with the ablated material, a laser beam operated in pulse mode was divided into two streams to ablate/excite the target sample in different directions instead of the conventional one beam excitation in single pulse LIBS (SP-LIBS). In spatial configuration, the laser beam geometry plays an important role in the emission signal enhancement. Thus, an adjustable geometric configuration with variable incident angle between the two splitted laser beams was constructed for achieving maximum signal enhancement. With the optimized angles of 60° and 70° for Al and Cu atomic emission lines at 396.15 nm and 324.75 nm respectively, about 5.6- and 4.8-folds signal enhancements were achieved for aluminum alloy and copper alloy samples compared to SP-LIBS. Furthermore, the temporal analysis, in which the intensity of atomic lines in SP-LIBS decayed at least ten times faster than the SBS-LIBS, proved that the energy coupling efficiency of SBS-LIBS was significantly higher than that of SP-LIBS.

Many traditional techniques for elemental analysis rely on use of plasmas to excite sample, and then the sample's composition can be identified and determined by atomic absorption spectroscopy (AAS) or atomic emission spectroscopy (AES). One of the AES-based techniques for elemental analysis is laser induced breakdown spectroscopy (LIBS), which is a powerful spectroscopic technique for direct analysis of various materials[1,2]. The method is based on focusing a high power laser radiation on a sample surface to form a plasma, and its emission is used to identify and quantify elements in solid[3–7], liquid[8–11], gaseous[12,13] and even aerosol[14–16] samples. One of the main advantages in LIBS is the simultaneous sampling and excitation, which can be achieved with a single laser pulse. Many solid samples can be analyzed directly or with minimal preparation, so LIBS shortens the full analysis cycle compared to most other analysis techniques[1,2,17]. Standard ICP or discharge based techniques must use background argon or other noble gases to perform analysis, which is not a necessary part for most LIBS experiments. The applications that can be benefited from the unique advantages of LIBS include environmental[18–20], industrial[21], geological[22–25], planetary[26,27], homeland security[28,29], and dental analysis[30].

In spite of the increasing popularity of LIBS, the processes involved in the laser-induced plasma formation, ablation, atomization, and excitation are complex and difficult to reproduce, leading to poor sensitivity, precision, and detection limits[31–33] compared to other forms of atomic spectroscopy such as inductively coupled plasma atomic emission spectroscopy (ICP-AES) or flame atomic emission spectroscopy. In order to improve the overall performance of LIBS, a significant amount of research to enhance the intensity of plasma emission based on combining different analytical techniques were investigated by different groups. For example, laser ablation has been coupled with additional excitation sources such as laser (dual-pulse LIBS)[34–36], microwave (microwave-assisted LIBS)[37,38], and hollow cathode lamp (spark-discharged LIBS)[39,40]. All of these techniques imply a non-negligible increase in complexity and cost of the LIBS set-up, although they succeeded in achieving improved limits of detection for the determination of many elements. Besides multiple excitation schemes, alternative methods based on spatially confining the plasma expansion[41,42] and easily ionizable elements (EIE-LIBS)[43] have

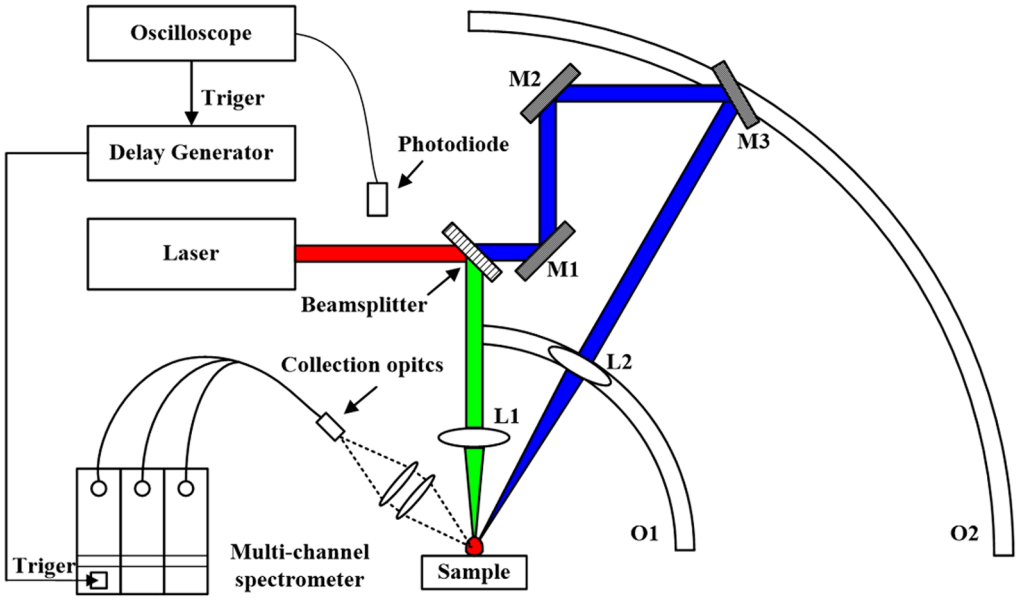

Figure 1 | Schematic diagram of experimental setup for the SBS-LIBS system. The centers of circular arc-shaped orbit 1 and 2 (O1, O2) were coincidence with the point that the reflection laser beam reached the sample. M1 and M2 were used to change the direction of the transmission laser, and M3 could be moved on the O1 for changing the angle of incident between reflection and transmission laser beams. L1 and L2 were used to focus laser beam on the sample surface.

been studied in order to enhance the intensity of plasma emission in single-pulse LIBS. Similar improvements have been made without the use of an additional excitation sources. However, the full analysis cycle is increased compared to standard LIBS due to complicated preparation procedure in these methods.

In this paper, we propose a new method for LIBS signal enhancement, in which the single-beam-splitting technique combined with a proper optical geometric configuration has been initially explored for effective signal enhancement with no requirement of an additional excitation source or a complicated preparation procedure of samples. In this approach, a laser pulse is divided into two laser beams to excite the sample from different directions instead of a single beam excitation in traditional LIBS. Additionally, the laser beam geometry plays an important role in the emission signal enhancement in SBS-LIBS. We here present an innovative geometric configuration, which is different from main beam geometries of dual-pulse LIBS, i.e., orthogonal and collinear configurations[34], to achieve the free adjustment of the incident angle of the two laser beams. To obtain maximum enhancements, the optimal angle between the two laser beams has been investigated. The optimum angle for the Al atomic emission line at 396.15 nm was found to be around 60° and approximately 70° for the Cu atomic emission line at 324.75 nm. Under these optimized conditions, the maximum enhancements of SBS-LIBS were found to be 5.6- and 4.8-fold for the copper and aluminum, respectively, relative to the signal obtained in traditional one single-pulse (SP) LIBS.

The experimental system of SBS-LIBS only adds a few optical lenses compared to standard LIBS. For this reason, the SBS-LIBS system should be more compact with lower cost compared to most other LIBS signal enhancement techniques, which would be useful for real-time and in situ analysis of solid sample, for example, food processing, medical applications, and Mars exploration program. To the best of our knowledge, this is the first report on LIBS signal enhancements using single-beam splitting technique.

Results

Geometric Configuration of SBS-LIBS design. The experimental setup for SBS-LIBS system was shown in Fig. 1. The initial laser pulse impinging at 45° on the surface of the beam-splitter (THORLABS BSW26) was optimized for 50 : 50 beam splitting for an angle of incidence (AOI) of 45°. The initial laser pulse was divided into a reflection and transmission laser beam by a beam-splitter. The reflection laser beam was aligned perpendicular to the sample surface and focused using a 50 mm focal length lens (L1,focal spot diameter ~10 μm,) such that the focal spot was formed at the sample surface. The transmission laser beam entered a set of optic lens consisting of three mirrors (M1, M2, M3), a 100 mm focal length lens (L2, focal spot diameter ~20 μm) and two circular arc-shaped orbits (O1, O2), and then reached the sample surface with an angle of β relative to the reflection laser.

The AOI between two laser beams could be changed within the range between 0~90° (except 0 and 90°) by adjusting M1, M2, M3 and L2 in this experimental setup (The specific adjustment procedure could be found in Method section). In the case of AOI = 0 (SBS-LIBS), the optical beam geometry was a collinear configuration[10], i.e., both beams propagate in the same direction and are delivered perpendicular to the sample surface. In the case of AOI = 90° (SBS-LIBS), The optical beam geometry was the similar with reheating configuration[44], i.e., the reflection laser beam was aligned perpendicular to the sample surface, and the transmission laser beam was aligned parallel to the sample surface, and was focused with a lens above the sample surface at 1 mm. The only difference was that the two laser beams in SBS-LIBS were splitted from one laser pulse, while the two laser beams in DP-LIBS were created by two independent lasers. For the single pulse setup, the beam splitter in Fig. 1 was exchanged with a reflection mirror.

In this experimental setup, both the reflection and transmission laser beams were produced by a single laser; therefore, the variation of the delay time, which was determined by their optical path difference (OPD), was very limited. In consideration of the energy attenuation and experimental complexity in SBS-LIBS, the OPD between two laser beams was less than 2.1 m, consequently, and the adjustment range of the delay time between the reflection and transmission laser beams was limited to 5.8~7.2 ns. The OPD and inter-beam delay in the different angles of incident (AOI) between two laser beams were listed in Table 1.

Assessment of coupling efficiency of laser energy to the ablated materials. It is well known that the signal intensities of LIBS can be

Table 1 | The OPD and inter-beam delay in the different angles of incident (AOI) between the two laser beams

AOI(degree)	OPD(m)	Inter-beam delay(ns)
0	1.70	5.80
10	1.85	6.31
20	1.98	6.75
30	2.07	7.06
40	2.10	7.16
50	2.10	7.16
60	2.07	7.06
70	1.98	6.75
80	1.85	6.31
90	1.70	5.80

enhanced by increasing the pulse energy of the laser. However, the enhancement effects of LIBS tend to be saturated at a certain value of laser energy, and further increasing the laser energy cannot bring obvious signal enhancement. To examine this phenomenon, we tested and identified the influence of emission intensities of Al I at 396.15 nm and Cu I at 324.75 nm through increasing laser energy. In order to avoid the strong continuous emission occurring during the SP processes, the spectral acquisitions were performed after a delay time of 2 μs from the laser pulse. The laser pulse energy was varied from 20 to 200 mJ. To better evaluate the SP coupling efficiency of laser energy to the ablated materials, the signal intensities in different pulse energy levels were normalized to the signal intensities with 200 mJ pulse energy. The emission spectra acquired for performing such survey were obtained by 3 ms gate of a CCD detector. As shown in Fig. 2, in the laser pulse energy range of 20 to 80 mJ, 80 to 140 mJ, and 140 to 200 mJ, Al line increased from 0 to 70.1%, 70.1% to 94.8%, and 94.8% to 100%, respectively. Similarly, the 324.75 nm Cu peak increased from 0 to 61.8%, 61.8% to 87.8%, and 87.8% to 100%, respectively. It can be noticed that the obvious increase of LIBS signal intensity has been observed when the laser pulse energy at relatively low level. On the contrary, the increase drops off quickly when laser pulse energy over 80 mJ.

The above phenomenon could be explained by the difference of coupling efficiency of laser energy to the ablated materials with the increased laser pulse energy. The plasma was weakly ionized when the laser energy was at a low level, and most energy of laser pulse was used for ablating the sample and ionizing the plasma, which were benefit for improving signal intensity. At high energy, the leading edge of the laser pulse had enough energy to complete the ionization of the plasma, while at the same time an absorption zone which was opaque to laser beam formed in the plasma, hence some energy in the trailing edge of the laser pulse was blocked by the absorption zone. Although the signal intensities increased with the improved laser pulse energy, the efficiency of laser energy coupled to the ablated materials was decreased when the laser energy was sufficiently high.

The signal enhancement in SBS-LIBS configuration. The Al I line at 396.15 nm and the Cu I line at 324.75 nm were chosen for spectral analysis due to their strong presence under our experimental conditions. Representative spectra for three experimental cases, specifically for SBS-LIBS with AOI of 30° and 60° along with the single-pulse only case, were shown in Fig. 3. A significant increase in both atomic emission line intensity and continuum emission intensity was recorded in all cases of SBS operation (upper and middle spectra) with respect to single laser pulse operation (lower spectra), as observed in Fig. 3. The peak intensity of the 396.15 nm Al line increased from a SP value of 7622 counts to a maximum value of 42608 counts at SBS-LIBS AOI of 60° in Fig. 3(a). Similarly, the 324.75 nm Cu peak intensity increased from a SP value of 6215 counts to a maximum value of 27324 at SBS-LIBS AOI of 60° in Fig. 3(b). Astoundingly, this result differs significantly from the previous studies that employed a pair of ns pulses for which no enhancements were observed in DP-LIBS configuration when the inter-pulse delay was at nanosecond level[45].

The SEM images in Fig. 4 show the craters produced using single-pulse and SBS-LIBS excitation, with 50 consecutive laser shots. Following ablation, the surface of sample in and around the ablation site was characterized by cracking and pitting, with the behavior observed for the SBS-LIBS increase. For SBS-LIBS configuration, Fig. 4 (b) and (c) show that the two laser beams were so precisely aligned that the two laser spots fall on one point on the sample surface.

The effect of inter-beam incident angle for signal enhancement in SBS-LIBS. In SBS-LIBS, the AOI between two laser beams plays an important role in signal enhancement. Therefore, we examined the

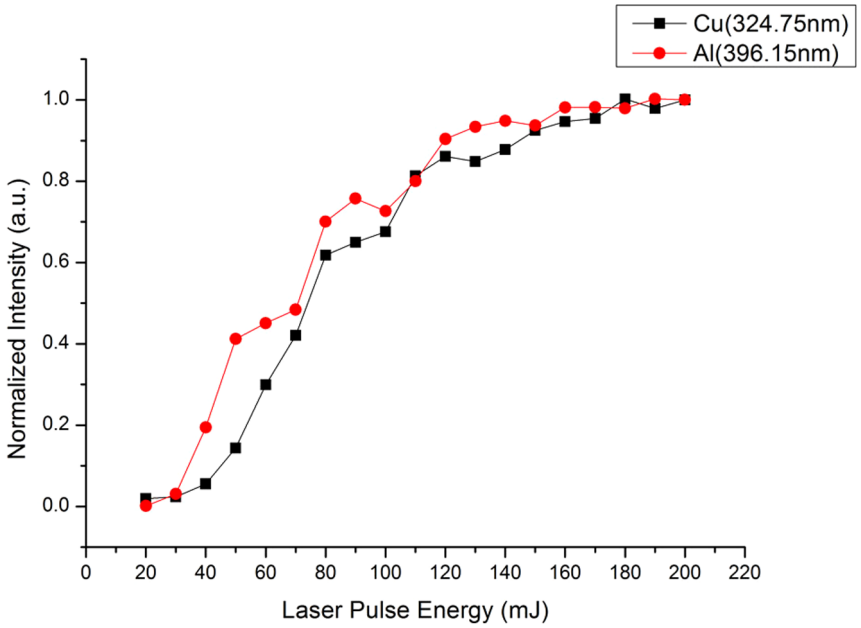

Figure 2 | The normalized intensity of the Cu I (324.75 nm) line and Al I (396.15 nm) line at different laser pulse energies.

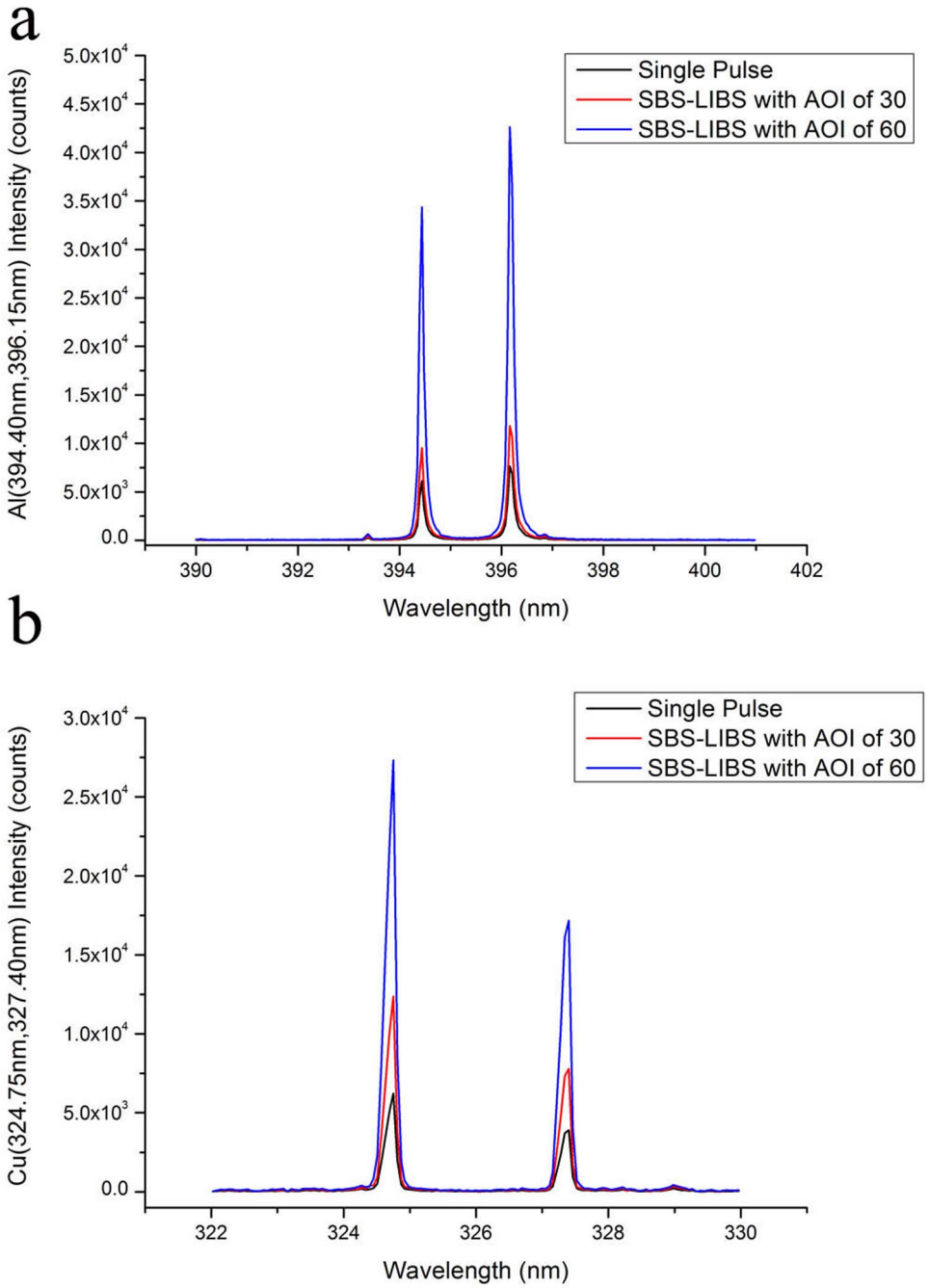

Figure 3 | Spectra showing atomic emission lines of interest, Al I at 396.15 nm and Cu I at 324.75 nm. The spectra correspond to single-pulse LIBS (lower spectrum), SBS-LIBS with AOI of 30° (middle spectrum), and SBS-LIBS with AOI of 60° (top spectrum). Line intensities were significantly enhanced.

emission signal intensities of the atomic lines of aluminum and copper by varying the inter-beam AOI from 0 to 90°. To quantify the increase in emission signals with the SBS-LIBS, the peak intensity and signal-to-background (S/B) ratios were calculated for both SBS and SP operations. To compare the data over the range of inter-beam AOI in SBS-LIBS, all the absolute peak intensity and S/B ratios were normalized to the respective SP value, as shown in Fig. 5. The raw peak intensity values increased by a maximum of 5.6-fold around AOI of 60° and 4.8-fold around AOI of 70° for Al and Cu emission lines, respectively. Because the continuum emission was also found to increase considerably with the SBS configuration, the resulting S/B ratio was less than the raw atomic emission peak intensities. Specifically, the S/B values are of 2.16- and 2.23-fold maximum for Al and Cu emission lines, respectively.

According to the above experiments, three key features should be noticed in the Fig. 5: firstly, a slight signal suppression at AOI = 0 and 10° was observed; secondly, the signal was enhanced by increasing inter-beam AOI in the range of 20∼70°; thirdly, the signal enhancement effect drops off quickly for inter-beam AOI > 70°. For the first observation (AOI = 0 and 10°), the reflection and transmission laser beams were acted like single pulse because the delay time between two laser beams was less than the initial laser pulse width. But this combined single pulse width was more than initial real single pulse because of inter-beam delay, resulting in a lessened peak power of laser pulse and analyte response as observed here.

To explain the second observation and identify the relationships between inter-beam AOI and the enhancement effect of signal

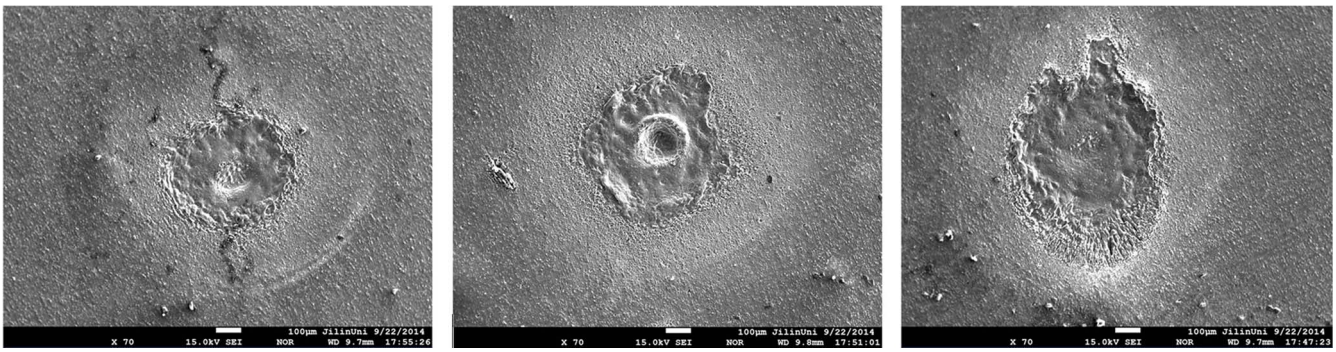

Figure 4 | SEM images of the ablation craters for an aluminum alloy sample using (a) SP-LIBS, and SBS-LIBS inter-beam AOI of (b) 30° and (c) 60°.

intensity in SBS-LIBS system, a plasma formation model on a plane surface was taken, as illustrated in Fig. 6. Most energy of trailing edge of the laser pulse was blocked by the absorption zone formed in the plasma when the laser pulse energy was significantly high, as described in the above experiment. Moreover, some studies indicate that the absorption zone was not uniform and diffused along the direction of the incident laser[1]. In the direction of incident laser, the thickness of the absorption zone reaches maximum, and

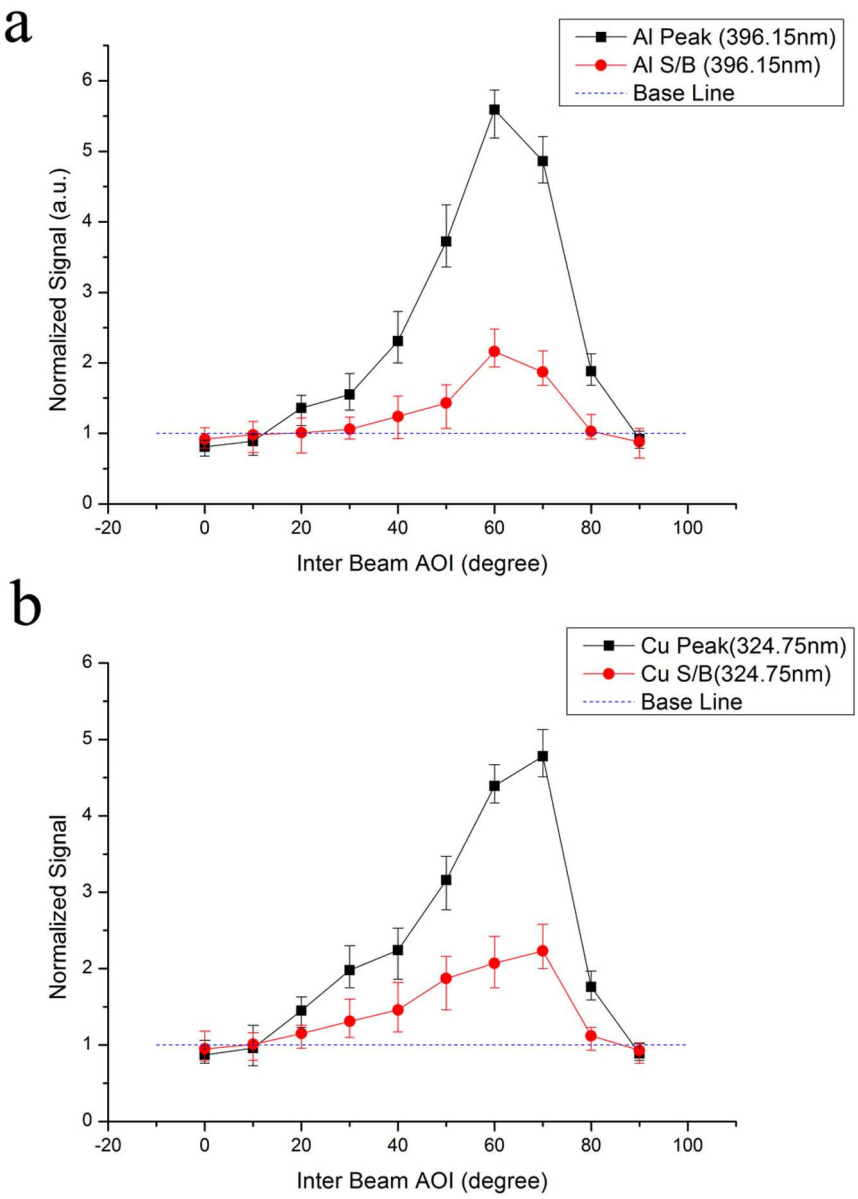

Figure 5 | Spectral atomic emission intensity (solid squares) and S/B ratio (solid circle) measurements as a function of the inter-beam AOI in SBS-LIBS. The values were normalized respective to the SP data. The Al I line at 396.15 nm (a) and the Cu I line at 324.75 nm (b) were selected for spectral analysis. The error bars show the standard deviation of 50 replicate measurements.

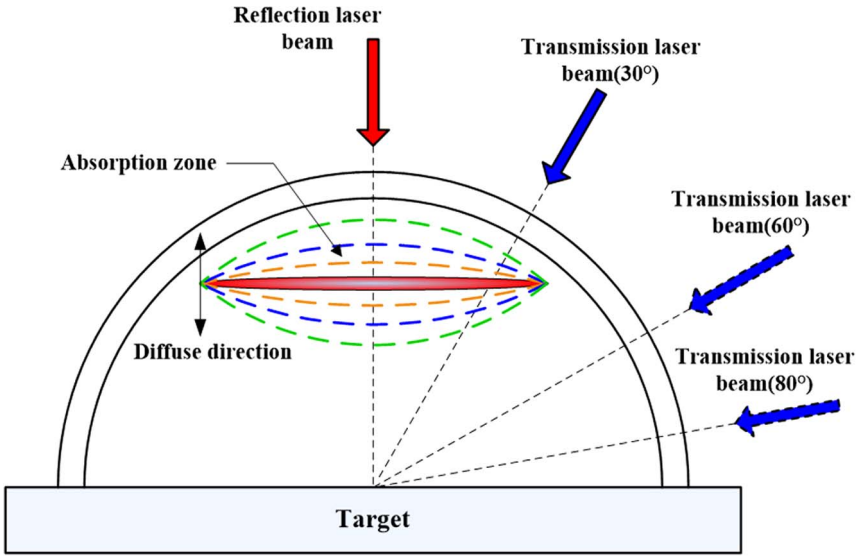

Figure 6 | Schematic diagram of the development of a laser plasma initiated on a plane solid surface. The reflection laser beam (red arrow) is directed orthogonal to the target surface, and the transmission laser beam (blue arrow) irradiates at an angle ranging from 0°~90° with respect to the axis of the reflection laser beam. The overlap of the absorption zone and the incident path of laser beam (black dash line) represent the thickness of absorption zone threaded by the transmission laser beam.

decreases with deviation from the incident laser beam. The thicker the absorption zone is, the more it consumes the laser energy. Therefore, the thickness of absorption zone threaded by the transmission laser beam decreased with the increasing inter-beam AOI, and more energy of transmission laser beam should be used to ablate samples.

For the third observation, the signal enhancement effect was significantly decreased when further increasing the inter-beam AOI.

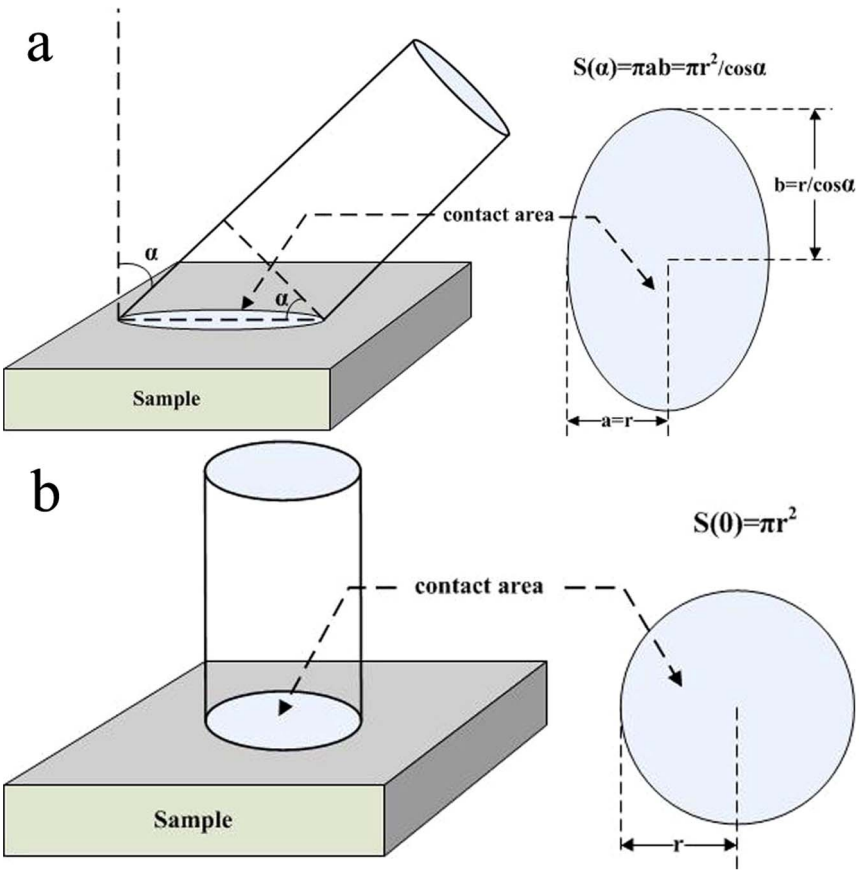

Figure 7 | Schematic diagram of the contact area of a transmission laser beam is incident to the sample surface. The contact area (a) is calculated by $S(\alpha) = \pi r^2/\cos\alpha$, where α is the angle of incident between reflection and transmission laser beams, r is the radius of transmission laser beam. The value of contact area (b) reaches minimum when the transmission laser beam is directed orthogonally to the target surface ($\alpha = 0$).

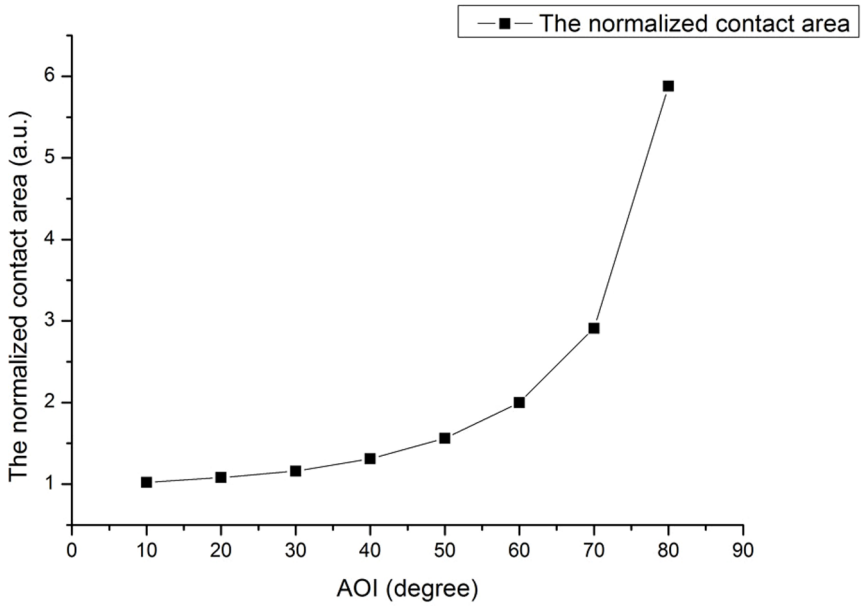

Figure 8 | The contact area between transmission laser beam and the sample surface as a function of the incident angle between reflection and transmission laser beams. Values are normalized to the minimum contact area ($S(\alpha)/S(0) = 1/\cos\alpha$).

The contact area between transmission laser beam and the sample surface would be significantly increased for inter-beam AOI more than 70°, the effectiveness of the laser energy per unit area could drop off quickly. Therefore, a short discussion of the effect of contact area between the transmission laser beam and the sample surface on signal enhancement is presented below: With the possible optical system error and the surface smoothness of the sample, the contact area should be considered as one of the reasons for performance evaluation, which can be calculated by the following formula:

$$S = \pi ab \tag{1}$$

where a and b is the minor axis and major axis of elliptical contact area, respectively, as shown in Fig. 7(a). According to the principles of trigonometry, a and b are equal to the radius of transmission laser beam r and $r/\cos\alpha$, respectively, thus, the formula of S can be rewritten in the following formula:

$$S(a) = \pi r^2 / \cos\alpha \tag{2}$$

where α is the angle of incident between reflection and transmission laser beams. The value of contact area reaches minimum when the transmission laser beam is directed orthogonal to the target surface ($\alpha = 0$), as observed in Fig. 7(b). To compare the data over the range of inter-beam AOI in SBS-LIBS, all the contact areas were normalized to the minimum contact area ($S(\alpha)/S(0) = 1/\cos\alpha$), as shown in Fig. 8.

The relationship between inter-beam delay and signal intensity in SBS-LIBS. As mentioned in **Geometric Configuration of SBS-LIBS**

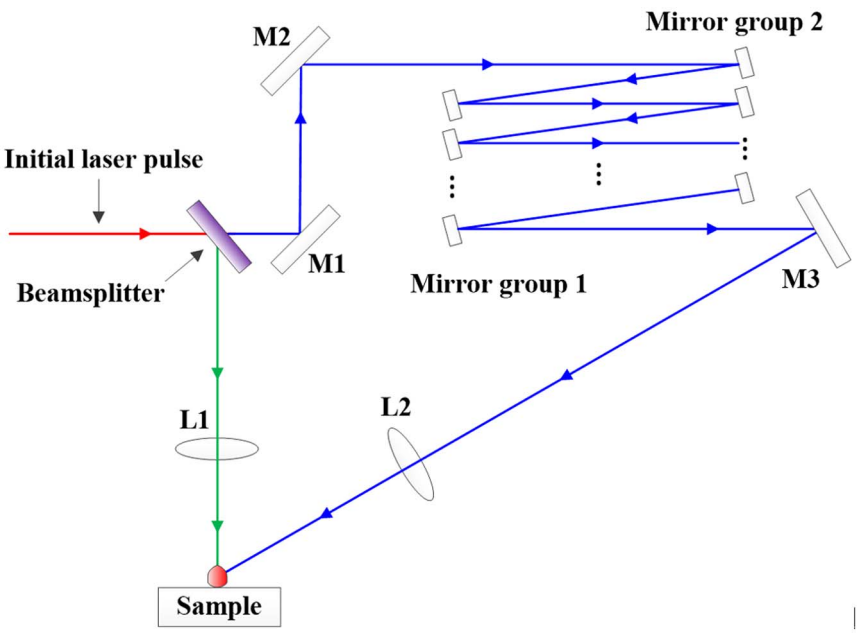

Figure 9 | Schematic diagrams of the optical beam geometry configuration for investigating the relationship between inter-beam delay and signal intensity in SBS-LIBS.

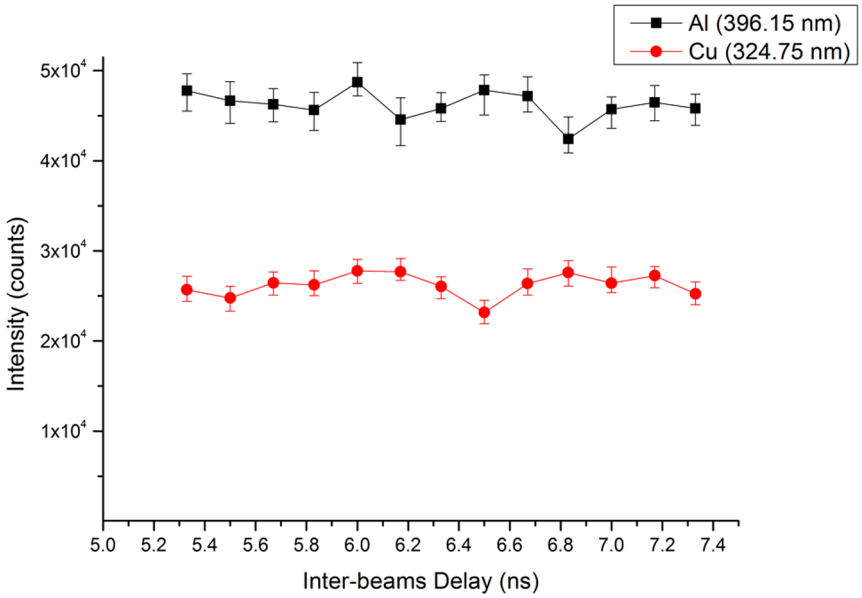

Figure 10 | Dependence of SBS-LIBS intensities of Al I line at 396.15 nm and Cu I line at 324.75 nm on inter-beam delay time.

design section, the delay time is different with inter-beam AOI changing. In order to investigate the relationship between inter-beam delay and signal intensity, the experimental setup is improved. As shown in the Fig. 9, the AOI was fixed at 60°,and the delay time was changed by using different number of mirrors in mirror groups 1 and 2. Fig. 10 shows a plot of the LIBS emission intensity versus inter-beam delay for the 396.15 nm Al line and 324.75 nm Cu line in the samples. Slight changes of signal intensity with different delay time were observed, which suggests the effect of inter-beam delay ranged from 5.3 to 7.3 ns on signal intensity could be insignificant with changing AOI.

Enhancement effect of SBS-LIBS at different laser pulse energies. In this experiment, the enhancement effect of signal intensity using SBS-LIBS configuration by varying the pulse energy of initial laser from 20 mJ to 200 mJ are investigated, with the inter-beam AOI in SBS-LIBS fixed at 60° for Al and 70° for Cu, respectively. The detector gate delay time and width were the same as in the above experiment. Fig. 11 shows the signal enhancement factor, S.E. (the ratio of signal emission intensities in the SP- and SBS-LIBS spectra). It should be noted that the enhancement effect of signal intensity was divided into three linear regions with the variation of the laser pulse energy.

In the first linear region (laser pulse energy ranging from 20 to 60 mJ), the signal intensity of SBS-LIBS was less than SP-LIBS for both Cu and Al analysis. The decreasing behavior of the emission intensity could be explained by the energy of each laser beam generated by the initial laser pulse, which was not much larger than the breakdown threshold. The observation in this region strongly suggests that the SBS-LIBS configuration was not suitable for signal enhancement using lower laser pulse energy. In the second linear region (laser pulse energy ranging from 60 to 160 mJ), the signal

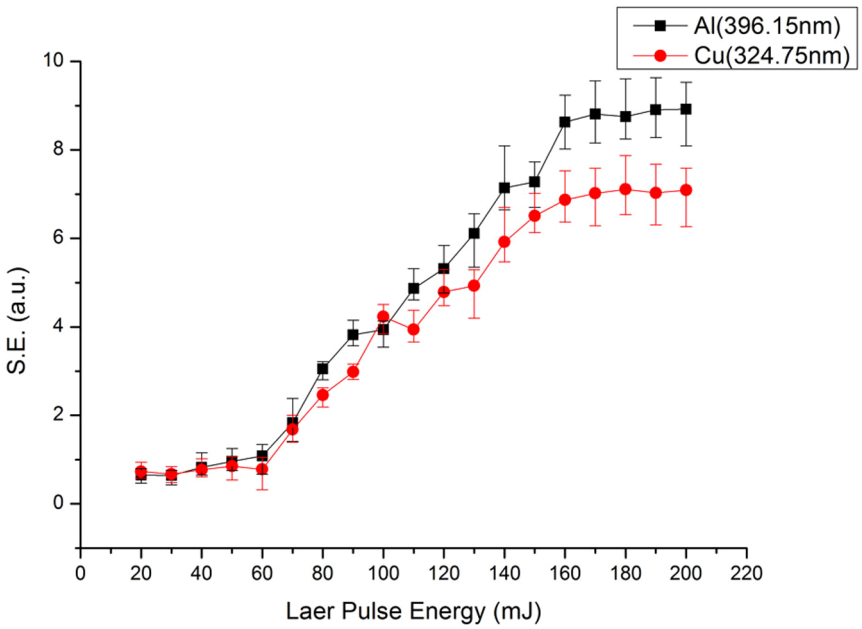

Figure 11 | The S.E. (the ratio of signal emission intensities in the SBS- and SP-LIBS spectra) as a function of laser pulse energy. The error bars show the standard deviation of 50 replicate measurements.

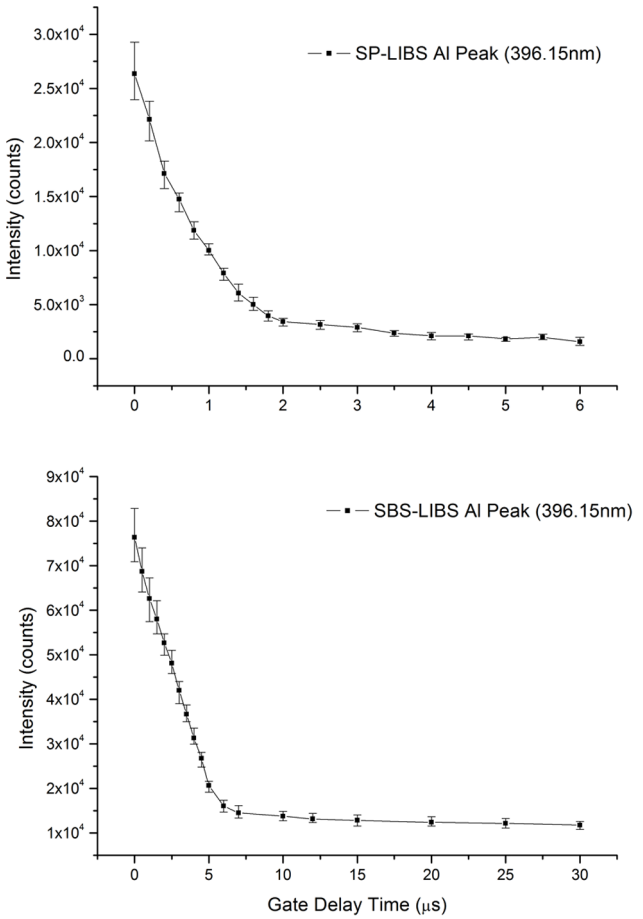

Figure 12 | Intensity of the 396.15 nm Al line versus decay time after the laser pulse using SP-LIBS (a) and SBS-LIBS (b) excitation. The laser pulse energy and gate width were fixed at 120 mJ and 3 ms, respectively, and the inter-beam AOI was 60° in SBS-LIBS configuration. The error bars show the standard deviation of 50 replicate measurements.

intensity was obviously enhanced by SBS-LIBS, because the coupling efficiency of laser energy to the ablated materials was significantly improved by using SBS-LIBS configuration when laser pulse energy at a relative high level. And the enhancement effect was improved with the increasing laser pulse energy. In the third linear region (laser pulse energy ranging from 160 to 200 mJ), since the energy of initial laser pulse was too high, the coupling efficiency of reflection and transmission laser energy to the ablated materials tend to be saturated, and further increasing the laser energy cannot bring significant change in signal enhancement. According to the principle of SBS-LIBS, theoretically we expect that further extension of the current SBS could be possible, which means multi-beam splitting mode from the initial laser pulse, divided into multi-beams, i.e., four beams, eight beams or even more, could be achievable for further improving coupling efficiency of laser energy to the ablated materials, provide the laser pulse is powerful enough. These multi-beam modes have not been yet tested in this work because of restrictions of our experimental conditions.

Temporal analysis for SBS-LIBS and SP-LIBS. Study of the attenuation rate for both SBS-LIBS and SP-LIBS cases were conducted in this work. The experiments to estimated temporal behaviors of the signal intensity occurring in both SP-LIBS and SBS-LIBS configurations were conducted. Kinetic spectral series with progressive delay time of 0.1 μs step from the first laser shot for SP-LIBS, or 0.5 μs step from the transmission laser beam for SBS-LIBS, were studied. Conversely, the detection system gate width was fixed at 3 ms in both cases. Fig. 12 shows a plot of the LIBS signal intensity versus detector gate delay. The results reported in Fig. 12(a) show that during the SP induced plasma the signal intensity was about 25000 counts in the first hundreds of ns and then rapidly drops down, after about 1.8∼2.0 μs, the SP induced plasma reaches a signal intensity plateau of 3500 counts. On the other hand, the SBS induced plasma line emission intensities last for roughly 30 μs and this is certainly due to its slow temporal decay of the plasma, as shown in Fig. 12(b), where the signal intensity remains at about 13000 counts even for a relatively long time delays (10.5∼12.0 μs). Therefore, it can be assumed that the plasma plume induced by reflection laser beam can efficiently be reheated by transmission laser beam of the SBS-LIBS configuration, sustaining for longer plasma lifetime.

Discussion

In this paper, we propose a new method for LIBS signal enhancement, in which the single-beam-splitting technique is combined with LIBS. In this approach, a laser pulse is divided into two laser beams to ablate and excite samples. To obtain maximum enhancements, the effect of inter-beam AOI on the emission signal intensity was investigated. The raw peak intensity values and S/B ratios increased 5.6- and 2.16- fold around AOI of 60° for Al I line at 396.15 nm, respectively, and increased 4.8- and 2.23- fold around AOI of 70° for Cu I line at 324.75 nm, respectively. One possibility is that an absorption zone generated by the leading edge of the laser pulse consumed most of the trailing edge of the laser pulse energy, resulting in decreased coupling of the ablation pulse to the sample surface in traditional SP-LIBS configuration. The absorption zone diffuses along the direction of the incident laser, and the thickness of absorption zone threaded by the transmission laser beam decreased with the increasing inter-beam AOI in SBS-LIBS, and more energy of transmission laser beam was used to ablate samples.

The proposed SBS-LIBS technology achieved the excitation of a sample using two laser beams; this technology is superficially similar to the widely reported DP-LIBS[34]. However, there are essential differences between these two technologies in terms of both realization method and signal enhancement principle. The signal enhancement principle of DP-LIBS technology can be divided into three modes: collinear[10], pre-ablation[46], and reheating[35,44]. The enhancement principle of collinear and reheating modes involved the direct bombardment on plasma for the second excitation by a second laser pulse when the first laser-produced plasma entered the decay phase[34], whereas the pre-ablation mode relied on a special environment of the sample surface formed by the first laser pulse such as shock-induced reduced pressure or thermal lensing caused by the pre-ablation laser spark[45]. The SBS-LIBS technology proposed in this paper changed the traditional LIBS excitation mode, and the energy of one laser pulse was dispersed into two directions for the sample excitation to increase the utilization efficiency of a single laser, thus achieving the enhancement of LIBS signal.

In terms of the implementation method, the two laser pulses in DP-LIBS were generated by two different lasers, and a synchronous machine was needed in DP-LIBS for the two laser pulses to generate a certain delay time to obtain the best signal enhancement[47]. The delay time was generally approximately three orders of magnitude higher than that of the laser pulse width of the first pulse[48]. For example, when femtosecond or nanosecond lasers were used for DP-LIBS excitation, the delay time to obtain the best signal enhancement was ps[49] and μs[45] levels, respectively. According to previous reports, when the delay time between two laser beams was less than 100 times of laser pulse width, the signal enhancement effect decreased significantly[44,45,47,48]. In this work, two laser beams could be obtained in the proposed SBS-LIBS technology by splitting a single pulse generated by one laser; thus, the interval time of the two laser beams reaching the sample surface was only determined by the OPD of two laser

beams (<10 ns). When the delay time between the two laser beams was short or none, the SBS-LIBS technology could still achieve the signal enhancement, which was impossible for the DP-LIBS technology.

The enhancement effect of signal intensity using SBS-LIBS configuration as a function of the laser pulse energy was investigated. We have found that the SBS-LIBS configuration was not suitable for signal enhancement when using lower laser pulse energy(less than 60 mJ). On the contrary, the obvious signal enhancement was obtained at high enough laser pulse energy (range from 60 to 160 mJ). However, the enhancement effect tended to be saturated when the laser pulse energy over 160 mJ. As a relevant remark, the SBS configuration used in this work showed a pretty slow lifetime temporal decay of the plasma, providing emission lines lasting longer than those occurring for SP-LIBS.

Methods

Procedures for inter-beam AOI adjustment. The experimental setup as shown in Fig. 1 needs to be adjusted with the AOI between reflection and transmission laser beams changing. The vertical distance between M3 and the sample surface can be defined by the following expression: $h_1 = R_1\cos\beta$, as well as the vertical distance between L2 and the sample surface can be defined by the following expression: $h_2 = R_2\cos\beta$, where β is the AOI between reflection and transmission laser beams, and R_1 and R_2 are the radius of O1 and O2, respectively. Also, the horizontal angles of the axis of M3 and L2 can be defined by the following expressions: $\alpha_1 = \frac{\pi - 2\beta}{4}$ and $\alpha_2 = \frac{\pi - 2\beta}{2}$, respectively. Thus M3 and L2 are able to be fixed at certain position on the O2 and O1, respectively. In the procedure for beam alignment, there may exist some tiny errors. In order to observe the exact position of the two laser spots clearly, a 532 nm continuous laser was used to replace the Nd:YAG laser for fine adjusting M1, M2, M3 and L2 in the system optimization process.

The experimental system parameters in detail. All the experiments were performed in open air at room temperature. A LOTIS TII 2131 M, Q-switched Nd: YAG laser operates at the fundamental wavelength of 1064 nm at a repetition rate of 1 Hz pulse.

The plasma emission was collimated and focused by a 50-mm fused-silica focal lens onto the entrance of fiber optic with a core diameter of 0.5 mm and fed into a three channel spectrometer (AvaSpec Multi-channel). Two 2400 groove/mm gratings were used for channels 1 and 2 to provide a wavelength range of 200–317 nm with a 0.10 nm spectral resolution and a wavelength range of 316–418 nm with a 0.10 nm spectral resolution, respectively. The third channel had the wavelength range of 415–930 nm with a 0.50 nm spectral resolution through the dispersion of a 1200 groove/mm grating.

In the experiment, the detector gate delay was varied from 0 to 50 μs with minimal jitter (15 ns) using a delay generator (Stanford Instruments Model DG535) after the initial laser beam. The time difference between the detector gate and initial laser beam was continuously monitored using a rapid photodiode (Newport, Model 818-BB-21) coupled with an oscilloscope (GWINSTEK GDS-2202A).

Safety hazard note. The laser (LOTIS TII 2131 M) is capable of emitting levels of both visible and invisible radiation that can cause damage to the eyes and skin, thus care should be taken in order to avoid hurt.

Sample introduction. The samples were aluminum alloy (91 wt.% Al) and copper alloy(90 wt.% Cu) which were mounted on a three-dimensional adjustable stage. Each point in the distributions was averaged over approximately 50 shots to minimize the effects on the LIBS spectra of stochastic fluctuations in the laser intensity, breakdown position, electronic noise, etc.

1. Cremers, D. A. & Radziemski, L. J. *Handbook of Laser-Induced Breakdown Spectroscopy* (John Wiley & Sons, Ltd London 2006).
2. Lin, Q., Niu, G., Wang, Q., Yu, Q. & Duan, Y. Combined Laser-Induced Breakdown with Raman Spectroscopy: Historical Technology Development and Recent Applications. *Appl Spectrosc Rev* **48**, 487–508 (2013).
3. Aragon, C., Penalba, F. & Aguilera, J. A. Spatial distributions of the number densities of neutral atoms and ions for the different elements in a laser induced plasma generated with a Ni-Fe-Al alloy. *Anal BioanalChem* **385**, 295–302 (2006).
4. Bousquet, B. *et al.* Development of a mobile system based on laser-induced breakdown spectroscopy and dedicated to in situ analysis of polluted soils. *Specrochim Acta B* **63**, 1085–1090 (2008).
5. Cunat, J., Fortes, F. J. & Laserna, J. J. Real time and in situ determination of lead in road sediments using a man-portable laser-induced breakdown spectroscopy analyzer. *Anal Chim Acta* **633**, 38–42 (2009).
6. Gottfried, J. L. *et al.* Laser-induced breakdown spectroscopy for detection of explosives residues: a review of recent advances, challenges, and future prospects. *Anal BioanalChem* **395**, 283–300 (2009).
7. Khumaeni, A. *et al.* A unique technique of laser-induced breakdown spectroscopy using transversely excited atmospheric CO2 laser for the sensitive analysis of powder samples. *Curr Appl Phys* **11**, 423–427 (2011).
8. Yun, J. I., Bundschuh, T., Neck, V. & Kim, J. I. Selective determination of europium(III) oxide and hydroxide colloids in aqueous solution by laser-induced breakdown spectroscopy. *Appl Spectrosc* **55**, 273–278 (2001).
9. Michel, A. P. M., Lawrence-Snyder, M., Angel, S. M. & Chave, A. D. Laser-induced breakdown spectroscopy of bulk aqueous solutions at oceanic pressures: evaluation of key measurement parameters. *Appl Opt* **46**, 2507–2515 (2007).
10. Lee, D-H., Han, S-C., Kim, T-H. & Yun, J-I. Highly Sensitive Analysis of Boron and Lithium in Aqueous Solution Using Dual-Pulse Laser-Induced Breakdown Spectroscopy. *Anal Chem* **83**, 9456–9461 (2011).
11. Lin, Q. *et al.* Laser-induced breakdown spectroscopy for solution sample analysis using porous electrospun ultrafine fibers as a solid-phase support. *RSC Adv* **4**, 14392–14399 (2014).
12. Sturm, V. & Noll, R. Laser-induced breakdown spectroscopy of gas mixtures of air, CO2, N-2, and C3H8 for simultaneous C, H, O, and N measurement. *Appl Opt* **42**, 6221–6225 (2003).
13. Hohreiter, V. & Hahn, D. W. Calibration effects for laser-induced breakdown spectroscopy of gaseous sample streams: Analyte response of gas-phase species versus solid-phase species. *Anal Chem* **77**, 1118–1124 (2005).
14. Martin, M. Z., Cheng, M. D. & Martin, R. C. Aerosol measurement by laser-induced plasma technique: A review. *Aerosol Sci Technol* **31**, 409–421 (1999).
15. Martin, M. & Cheng, M. D. Detection of chromium aerosol using time-resolved laser-induced plasma spectroscopy. *Appl Spectrosc* **54**, 1279–1285 (2000).
16. Wang, X., Shi, L., Lin, Q., Zhu, X. & Duan, Y. Simultaneous and sensitive analysis of Ag(i), Mn(ii), and Cr(iii) in aqueous solution by LIBS combined with dispersive solid phase micro-extraction using nano-graphite as an adsorbent. *J Anal At Spectrom* **29**, 1098 (2014).
17. Sivakumar, P., Taleh, L., Markushin, Y. & Melikechi, N. Packing density effects on the fluctuations of the emission lines in laser-induced breakdown spectroscopy. *Specrochim Acta B* **92**, 84–89 (2014).
18. Kasem, M. A., Russo, R. E. & Harith, M. A. Influence of biological degradation and environmental effects on the interpretation of archeological bone samples with laser-induced breakdown spectroscopy. *J Anal At Spectrom* **26**, 1733–1739 (2011).
19. Lei, W. *et al.* Time-resolved characterization of laser-induced plasma from fresh potatoes. *Specrochim Acta B* **64**, 891–898 (2009).
20. Boueri, M. *et al.* Identification of Polymer Materials Using Laser-Induced Breakdown Spectroscopy Combined with Artificial Neural Networks. *Appl Spectrosc* **65**, 307–314 (2011).
21. Noll, R. *et al.* Laser-induced breakdown spectrometry - applications for production control and quality assurance in the steel industry. *Specrochim Acta B* **56**, 637–649 (2001).
22. Harmon, R. S. *et al.* LIBS analysis of geomaterials: Geochemical fingerprinting for the rapid analysis and discrimination of minerals. *Appl Geochem* **24**, 1125–1141 (2009).
23. Diaz Pace, D. M. *et al.* Analysis of Minerals and Rocks by Laser-Induced Breakdown Spectroscopy. *Spectrosc Lett* **44**, 399–411 (2011).
24. Rakovsky, J. *et al.* Testing a portable laser-induced breakdown spectroscopy system on geological samples. *Specrochim Acta B* **74–75**, 57–65 (2012).
25. Zhu, X. *et al.* Advanced statistical analysis of laser-induced breakdown spectroscopy data to discriminate sedimentary rocks based on Czerny-Turner and Echelle spectrometers. *Specrochim Acta B* **93**, 8–13 (2014).
26. Colao, F. *et al.* Investigation of LIBS feasibility for in situ planetary exploration: An analysis on Martian rock analogues. *Planet Space Sci* **52**, 117–123 (2004).
27. Dyar, M. D. *et al.* Remote laser-induced breakdown spectroscopy analysis of East African Rift sedimentary samples under Mars conditions. *Chem Geol* **294**, 135–151 (2012).
28. Harmon, R. S. *et al.* Laser-induced breakdown spectroscopy - An emerging chemical sensor technology for real-time field-portable, geochemical, mineralogical, and environmental applications. *Appl Geochem* **21**, 730–747 (2006).
29. Gottfried, J. L., De Lucia, F. C., Jr., Munson, C. A. & Miziolek, A. W. Strategies for residue explosives detection using laser-induced breakdown spectroscopy. *J Anal At Spectrom* **23**, 205–216 (2008).
30. Celen, S. & Ozden, H. Laser-induced novel patterns: As smart strain actuators for new-age dental implant surfaces. *Appl Surf Sci* **263**, 579–585 (2012).
31. Telle, H. H., Beddows, D. C. S., Morris, G. W. & Samek, O. Sensitive and selective spectrochemical analysis of metallic samples: the combination of laser-induced breakdown spectroscopy and laser-induced fluorescence spectroscopy. *Specrochim Acta B* **56**, 947–960 (2001).
32. Guo, L. B. *et al.* Optimally enhanced optical emission in laser-induced breakdown spectroscopy by combining spatial confinement and dual-pulse irradiation. *Opt Express* **20**, 1436–1443 (2012).
33. Kuzuya, M. & Aranami, H. Analysis of a high-concentration copper in metal alloys by emission spectroscopy of a laser-produced plasma in air at atmospheric pressure. *Specrochim Acta B* **55**, 1423–1430 (2000).
34. Babushok, V. I. *et al.* Double pulse laser ablation and plasma: Laser induced breakdown spectroscopy signal enhancement. *Specrochim Acta B* **61**, 999–1014 (2006).

35. Coons, R. W., Harilal, S. S., Hassan, S. M. & Hassanein, A. The importance of longer wavelength reheating in dual-pulse laser-induced breakdown spectroscopy. *Appl Phys B-Laser O* **107**, 873–880 (2012).
36. Jiang, X., Hayden, P., Laasch, R., Costello, J. T. & Kennedy, E. T. Inter-pulse delay optimization in dual-pulse laser induced breakdown vacuum ultraviolet spectroscopy of a steel sample in ambient gases at low pressure. *Specrochim Acta B* **86**, 66–74 (2013).
37. Liu, Y., Baudelet, M. & Richardson, M. Elemental analysis by microwave-assisted laser-induced breakdown spectroscopy: Evaluation on ceramics. *J Anal At Spectrom* **25**, 1316–1323 (2010).
38. Ikeda, Y. & Tsuruoka, R. Characteristics of microwave plasma induced by lasers and sparks. *Appl Opt* **51**, B183–B191 (2012).
39. Nassef, O. A. & Elsayed-Ali, H. E. Spark discharge assisted laser induced breakdown spectroscopy. *Specrochim Acta B* **60**, 1564–1572 (2005).
40. Li, X., Zhou, W., Li, K., Qian, H. & Ren, Z. Laser ablation fast pulse discharge plasma spectroscopy analysis of Pb, Mg and Sn in soil. *Opt Commun* **285**, 54–58 (2012).
41. Popov, A. M., Colao, F. & Fantoni, R. Spatial confinement of laser-induced plasma to enhance LIBS sensitivity for trace elements determination in soils. *J Anal At Spectrom* **25**, 837–848 (2010).
42. Guo, L. B. *et al.* Plasma confinement by hemispherical cavity in laser-induced breakdown spectroscopy. *Appl Phys Lett* **98**, 131501(1–3) (2011).
43. Zhang, L-J., Chen, J-Z., Yang, S-P., Wei, Y-H. & Guo, Q-L. Enhancing Effect of Sample Additive on Laser-Induced Plasma Radiation. *Spectrosc Spec Anal* **30**, 1175–1178 (2010).
44. Santagata, A. *et al.* Femtosecond/Nanosecond dual-pulse orthogonal geometry plasma plume reheating for compositional analysis of ancient copper-based-alloy artworks. In: *COLA'05: 8th International Conference on Laser Ablation* (ed (eds Hess WP, Herman PR, Bauerle D, Koinuma H) (2007).
45. Hohreiter, V. & Hahn, D. W. Dual-pulse laser induced breakdown spectroscopy: Time-resolved transmission and spectral measurements. *Specrochim Acta B* **60**, 968–974 (2005).
46. Stratis, D. N., Eland, K. L. & Angel, S. M. Enhancement of aluminum, titanium, and iron in glass using pre-ablation spark dual-pulse LIBS. *Appl Spectrosc* **54**, 1719–1726 (2000).
47. Stratis, D. N., Eland, K. L. & Angel, S. M. Effect of pulse delay time on a pre-ablation dual-pulse LIBS plasma. *Appl Spectrosc* **55**, 1297–1303 (2001).
48. Scaffidi, J. *et al.* Dual-pulse laser-induced breakdown spectroscopy with combinations of femtosecond and nanosecond laser pulses. *Appl Opt* **42**, 6099–6106 (2003).
49. Semerok, A. & Dutouquet, C. Ultrashort double pulse laser ablation of metals. *Thin Solid Films* **453**, 501–505 (2004).

Acknowledgments

The authors are grateful to the financial support from the National Major Scientific Instruments and Equipment Development Special Funds (No. 2011YQ030113).

Author contributions

G.Y., Q.L., Y.D. and Y.D. conceived the original idea. G.Y. designed and executed the experiment under the guidance of Y.D. Finally, G.Y., Q.L., Y.D., D.T. and Y.D. analyzed the results and wrote the paper.

Additional information

Competing financial interests: The authors declare no competing financial interests.

How to cite this article: Yang, G., Lin, Q., Ding, Y., Di Tian & Duan, Y. Laser Induced Breakdown Spectroscopy Based on Single Beam Splitting and Geometric Configuration for Effective Signal Enhancement. *Sci. Rep.* **5**, 7625; DOI:10.1038/srep07625 (2015).